ANESTHESIOLOGY

Causes of Hypoxemia in COVID-19 Acute Respiratory Distress Syndrome: A Combined Multiple Inert Gas Elimination Technique and Dual-energy Computed Tomography Study

Mattia Busana, M.D., Anna Rau, M.D., Stefano Lazzari, M.D., Simone Gattarello, M.D., Massimo Cressoni, M.D., Lorenz Biggemann, M.D., Lars-Olav Harnisch, M.D., Lorenzo Giosa, M.D., Andreas Vogt, M.D., Leif Saager, M.D., Joachim Lotz, M.D., Birgit Meller, M.D., Konrad Meissner, M.D., Luciano Gattinoni, M.D., Onnen Moerer, M.D.

ANESTHESIOLOGY 2024; 140:251–60

EDITOR'S PERSPECTIVE

What We Already Know about This Topic

- Although different mechanisms of hypoxemia in COVID-19 acute respiratory distress syndrome (ARDS) have been suggested, there is ongoing debate regarding the underlying pathophysiology
- The multiple inert gas elimination technique (MIGET) and dual-energy computed tomography (DECT) are state-of-the art methods to analyze the functional and anatomical substrate of lung disease

What This Article Tells Us That Is New

- The authors found shunt, ventilation–perfusion mismatch, and potentially diffusion limitation or postpulmonary shunting in COVID-19 ARDS
- The authors also found an excess of blood volume compared to the tissue in well-aerated regions but not with atelectasis
- The findings support the concept of a multifactorial genesis of hypoxemia, in which alveolar factors, typical of ARDS, are combined with vascular factors, more typical of pulmonary embolism, all of which contribute to the overall severity of the disease

ABSTRACT

Background: Despite the fervent scientific effort, a state-of-the art assessment of the different causes of hypoxemia (shunt, ventilation–perfusion mismatch, and diffusion limitation) in COVID-19 acute respiratory distress syndrome (ARDS) is currently lacking. In this study, the authors hypothesized a multifactorial genesis of hypoxemia and aimed to measure the relative contribution of each of the different mechanism and their relationship with the distribution of tissue and blood within the lung.

Methods: In this cross-sectional study, the authors prospectively enrolled 10 patients with COVID-19 ARDS who had been intubated for less than 7 days. The multiple inert gas elimination technique (MIGET) and a dual-energy computed tomography (DECT) were performed and quantitatively analyzed for both tissue and blood volume. Variables related to the respiratory mechanics and invasive hemodynamics (PiCCO [Getinge, Sweden]) were also recorded.

Results: The sample (51 ± 15 yr; Pao_2/Fio_2, 172 ± 86 mmHg) had a mortality of 50%. The MIGET showed a shunt of 25 ± 16% and a dead space of 53 ± 11%. Ventilation and perfusion were mismatched (LogSD, Q, 0.86 ± 0.33). Unexpectedly, evidence of diffusion limitation or postpulmonary shunting was also found. In the well aerated regions, the blood volume was in excess compared to the tissue, while the opposite happened in the atelectasis. Shunt was proportional to the blood volume of the atelectasis (R^2 = 0.70, P = 0.003). $\dot{V}_A/\dot{Q}_T$ mismatch was correlated with the blood volume of the poorly aerated tissue (R^2 = 0.54, P = 0.016). The overperfusion coefficient was related to Pao_2/Fio_2 (R^2 = 0.66, P = 0.002), excess tissue mass (R^2 = 0.84, P < 0.001), and $Etco_2/Paco_2$ (R^2 = 0.63, P = 0.004).

Conclusions: These data support the hypothesis of a highly multifactorial genesis of hypoxemia. Moreover, recent evidence from post-mortem studies (*i.e.*, opening of intrapulmonary bronchopulmonary anastomosis) may explain the findings regarding the postpulmonary shunting. The hyperperfusion might be related to the disease severity.

(ANESTHESIOLOGY 2024; 140:251–60)

Since the beginning of the pandemic, a substantial scientific effort has been devoted to understanding the peculiar aspects of the derangement of gas exchange physiology in acute respiratory distress syndrome (ARDS) from COVID-19. Traditionally, hypoxemia can arise from shunt, in which the mixed venous blood does not directly come in

This article is featured in "This Month in ANESTHESIOLOGY," page A1. This article is accompanied by an editorial on p. 186. This article has a related Infographic on p. A17. Supplemental Digital Content is available for this article. Direct URL citations appear in the printed text and are available in both the HTML and PDF versions of this article. Links to the digital files are provided in the HTML text of this article on the Journal's Web site (www.anesthesiology.org). This article has an audio podcast. This article has a visual abstract available in the online version. Part of the work presented in this article was presented at the 2023 Association of University Anesthesiologists–International Anesthesia Research Society Meeting in Denver, Colorado, April 13 to 17, 2023.

Submitted for publication June 6, 2023. Accepted for publication August 9, 2023. Published online first on September 1, 2023.

Mattia Busana, M.D.: Department of Anesthesiology, University Medical Center of Göttingen, Göttingen, Germany.

 ANESTHESIOLOGY 2024; 140:251–60. DOI: 10.1097/ALN.0000000000004757

contact with alveolar gas; ventilation–perfusion ($\dot{V}_A/\dot{Q}_T$) mismatch, in which the relationship between ventilation and perfusion differs from 1:1 and the ratio might even be heterogeneous within the lung; and diffusion limitation, in which the venous blood does not reach the complete equilibration with the alveolar gas at the end of the pulmonary capillary. In ARDS, the hypoxemia is mainly due to shunt through the atelectasis.[1] A large body of evidence, however, shows that the alterations of the pulmonary vascularity are particularly prominent in COVID-19,[2] and therefore, it could be hypothesized that the pathogenesis of oxygenation impairment, in this case, might be more complex than what has been traditionally described for ARDS.[3] In the current study, we aimed to understand what is the relative contribution of the different mechanisms of hypoxemia in COVID-19 ARDS and what is the relationship between the alterations of ventilation and perfusion and the anatomical distribution of air, tissue, and blood within the lung.

Methods

Study Participants

The data reporting follows the Strengthening the Reporting of Observational Studies in Epidemiology (STROBE) guidelines for cohort observational studies. The study was approved by the hospital ethical board, registered (Deutsches Register Klinischer Studien DRKS00025503), and conducted in the intensive care unit of the University Medical Center of Göttingen (Germany). The only inclusion criteria was the diagnosis of ARDS[4] from COVID-19. The diagnosis of COVID-19 infection was confirmed with an RT-PCR test performed on a nasal swab. The measurements were performed within 7 days from the endotracheal intubation. Exclusion criteria were pregnancy, hepatic cirrhosis, extracorporeal membrane oxygenation, and patent foramen ovale. Patent foramen ovale was excluded with an agitated saline bubbles bolus during transthoracic echocardiography. The recruitment of patients ran from November 2021 to March 2022. The written informed consent was acquired from a patient's legal representative.

Measurements

A femoral or brachial artery was cannulated with a 4F PiCCO catheter (Getinge, Sweden). We recorded respiratory mechanics and hemodynamic data after PiCCO calibration. The cardiac output was measured by transpulmonary thermodilution. Samples for the MIGET were taken in duplicate from mixed expired gas and arterial blood, as explained below, together with an arterial and central venous blood gas analysis. After the measurement, the patient was transported to the computed tomography scan facility within 5 h. For technical and safety reasons, it was not possible to perform the whole measurement in the computed tomography scanner.

Multiple Inert Gas Elimination Technique (MIGET)

Six inert gases, namely sulfur hexafluoride-SF6, ethane, and cyclopropane (Air Liquide, Germany); isoflurane (Baxter, USA); diethyl ether and acetone (Merck, Germany), were dissolved in 500 ml of 0.9% NaCl (Baxter), before the measurement.[5,6] The infusion rate was set at 1/1,000 of the patient's minute ventilation. During the infusion, the ventilator circuit was modified, substituting the entire expiratory limb with a specifically designed 1-l, baffled, flow-through mixing box, heated above body temperature from the mouth opening to the gas sampling point.[7] After 30 min, an arterial blood sample and a time-aligned sample of the mixed expired gas were collected into ungreased, glass gastight syringes (Cadence Science, USA). The subsequent preparation of the samples (adapted to our own setup) is detailed in the supplemental digital content (https://links.lww.com/ALN/D303). The prepared probes were sent to the gas chromatography facility, and the data obtained were entered into the Fortran software kindly provided by Peter D. Wagner, M.D. (University of California, San Diego). Finally, the $\dot{V}_A/\dot{Q}_T$ distributions were recovered.

Anna Rau, M.D.: Department of Anesthesiology, University Medical Center of Göttingen, Göttingen, Germany.

Stefano Lazzari, M.D.: Department of Anesthesiology, University Medical Center of Göttingen, Göttingen, Germany; and Institute for Treatment and Research San Raffaele Scientific Institute, Department of Anesthesia and Intensive Care, Milan, Italy.

Simone Gattarello, M.D.: Department of Anesthesiology, University Medical Center of Göttingen, Göttingen, Germany; and Institute for Treatment and Research San Raffaele Scientific Institute, Department of Anesthesia and Intensive Care, Milan, Italy.

Massimo Cressoni, M.D.: Unit of Radiology, Institute for Treatment and Research Policlinico San Donato, Milan, Italy.

Lorenz Biggemann, M.D.: Institute for Diagnostic and Interventional Radiology, University Medical Center of Göttingen, Göttingen, Germany.

Lars-Olav Harnisch, M.D.: Department of Anesthesiology, University Medical Center of Göttingen, Göttingen, Germany.

Lorenzo Giosa, M.D.: Centre for Human and Applied Physiological Sciences, King's College London, London, United Kingdom.

Andreas Vogt, M.D.: Department of Anaesthesiology and Pain Medicine, Bern University Hospital, University of Bern, Bern, Switzerland.

Leif Saager, M.D.: Department of Anesthesiology, University Medical Center of Göttingen, Göttingen, Germany; and Outcomes Research Consortium, Cleveland, Ohio.

Joachim Lotz, M.D.: Institute for Diagnostic and Interventional Radiology, University Medical Center of Göttingen, Göttingen, Germany.

Birgit Meller, M.D.: Clinic of Nuclear Medicine, University Medical Center of Göttingen, Göttingen, Germany.

Konrad Meissner, M.D.: Department of Anesthesiology, University Medical Center of Göttingen, Göttingen, Germany.

Luciano Gattinoni, M.D.: Department of Anesthesiology, University Medical Center of Göttingen, Göttingen, Germany.

Onnen Moerer, M.D.: Department of Anesthesiology, University Medical Center of Göttingen, Göttingen, Germany.

Dual-Energy Computed Tomography (DECT)

The PiCCO was once more calibrated. DECT was carried out with the same ventilatory setup the patient had during MIGET. DECT was performed with a dual-source spiral unit (Siemens Somatom Force, Siemens Healthcare, Germany) at two different energy levels, after contrast injection.[8] The threshold for the bolus trigger was 120 HU, the injection rate was 3 ml/s, 5 seconds of delay before scanning. The scan was performed with bolus-tracking. From the study, we extracted two Digital Imaging and COmmunications in Medicine (DICOM) series through a three material mass fraction decomposition (syngo.via, Siemens Healthcare): a virtual unenhanced and a perfusion map. Each slice was manually contoured along the lungs, excluding the great vessels and bronchi. On the virtual unenhanced series, we performed a quantitative analysis as previously described.[9] The analysis carried out on the perfusion map is detailed in the supplemental digital content (https://links.lww.com/ALN/D303).[10] From -1000 HU to +100 HU, for each interval of 100 HU, we calculated fractions of the total for tissue and the blood volumes and the ratio between them. Summing these ratios, in those regions where this ratio was less than 1, led to the calculation of the overperfusion coefficient. Finally, a radiologist consultant (L.B.) diagnosed the presence of pulmonary embolism.

Statistical Analysis

A formal sample size has not been calculated a priori. We chose to enroll patients during what we hypothesized to be a "winter wave" of COVID-19, namely between November 2021 and March 2022. Given the stringent entry criteria, and the nature of our institution, we aimed to recruit between 10 to 15 patients.

The normal distribution of the variables was assessed with the Shapiro–Wilk test. The data are presented as means ± SD or medians [interquartile range] as appropriate. The quantitative relationship between variables was assessed with linear regression with the ordinary least-squares method. Two-tailed P values < 0.05 were considered statistically significant. The data analysis was performed in Julia 1.8[11] and the following packages: DataFrames.jl[12], Makie.jl[13], GLM.jl[14], and Distributions.jl[15].

Results

Study Sample

Between November 2021 and March 2022, 12 patients were eligible for inclusion. Two patients were excluded because of relevant patent foramen ovale (n = 1; table E1 supplemental digital content, https://links.lww.com/ALN/D303) and technical problems during the measurement (n = 1). A demographic characterization of the resulting sample (n = 10) is presented in table 1 and table E2 (supplemental digital content, https://links.lww.com/ALN/D303). Nine patients were infected with B.1.617.2 (Delta variant of COVID-19), one was infected with B.1.1.529 (Omicron variant), and only two were partially vaccinated (single dose). The laboratory analysis showed D-dimer elevation as commonly observed in COVID-19 (table E3, supplemental digital content, https://links.lww.com/ALN/D303). Table 1 also displays common respiratory and invasive hemodynamic variables measurable at the bedside.

Table 1. Anthropometric and Clinical Variables

Variable	Population (n = 10)
Demographics and outcome	
Age, yr	51 ± 15
Female, n, %	5, 50%
Body mass index, kg/m^2	30 ± 7
Time from symptoms, days	12 [10 to 15]
Time from intubation, days	4 [2 to 6]
ICU length of stay, days	16 [10 to 28]
ECMO after study, n, %	3, 30%
ICU mortality, n, %	5, 50.0%
Hemodynamics	
Heart rate, beats/min	75 ± 15
Mean arterial pressure, mmHg	84 ± 12
Cardiac index, l · min^{-1} · m^{-2}	3.13 ± 0.63
Systemic vascular resistance index, dyn · s · cm^{-5} · m^2	1,989 ± 401
Stroke volume variation, %	13 ± 7
Extravascular lung water index, ml/kg	14.7 [12.3 to 19.0]
Global end-diastolic volume, ml	1,213 ± 367
Ventilation settings and gas exchange	
Tidal volume, ml/kg	6.8 ± 2.0
Respiratory rate, breaths/min	20.2 ± 7.9
Positive end-expiratory pressure, cm H_2O	10 [9 to 11]
Pa_{O_2}/F_{IO_2}, mmHg	172 ± 86
Alveolo-arterial P_{O_2} difference, mmHg	289 ± 156
ET_{CO_2}, mmHg	41 ± 9
Ventilatory ratio	1.48 ± 0.43

The data are presented as means ± SD or medians [interquartile range] as appropriate.

ECMO, extracorporeal membrane oxygenation; Et_{CO_2}, end-tidal carbon dioxide; F_{IO_2}, fraction of inspired oxygen; ICU, intensive care unit.

Measurement of the Ventilation–Perfusion Distribution

The $\dot{V}_A/\dot{Q}_T$ distribution of each patient is represented in figure 1, while in figure E1 (supplemental digital content, https://links.lww.com/ALN/D303) are presented the plots of the retention–excretion of the inert gases. As shown, the patients presented with overall heterogeneous patterns of $\dot{V}_A/\dot{Q}_T$ alterations. The residual sum of square of the gas data fitting procedure was 4.7 [3.5 to 6.9], ensuring that MIGET was overall well performed. More than 50% of the cardiac output was distributed in regions with a $\dot{V}_A/\dot{Q}_T$ ratio between 0.1 and 1, while ventilation was more widely distributed among ratios 0.1 to 10. Both the scattering of perfusion (logarithm of the SD, LogSD, Q) and the one of ventilation (LogSD, V) were abnormal, indicating a relevant presence of $\dot{V}_A/\dot{Q}_T$ mismatch.

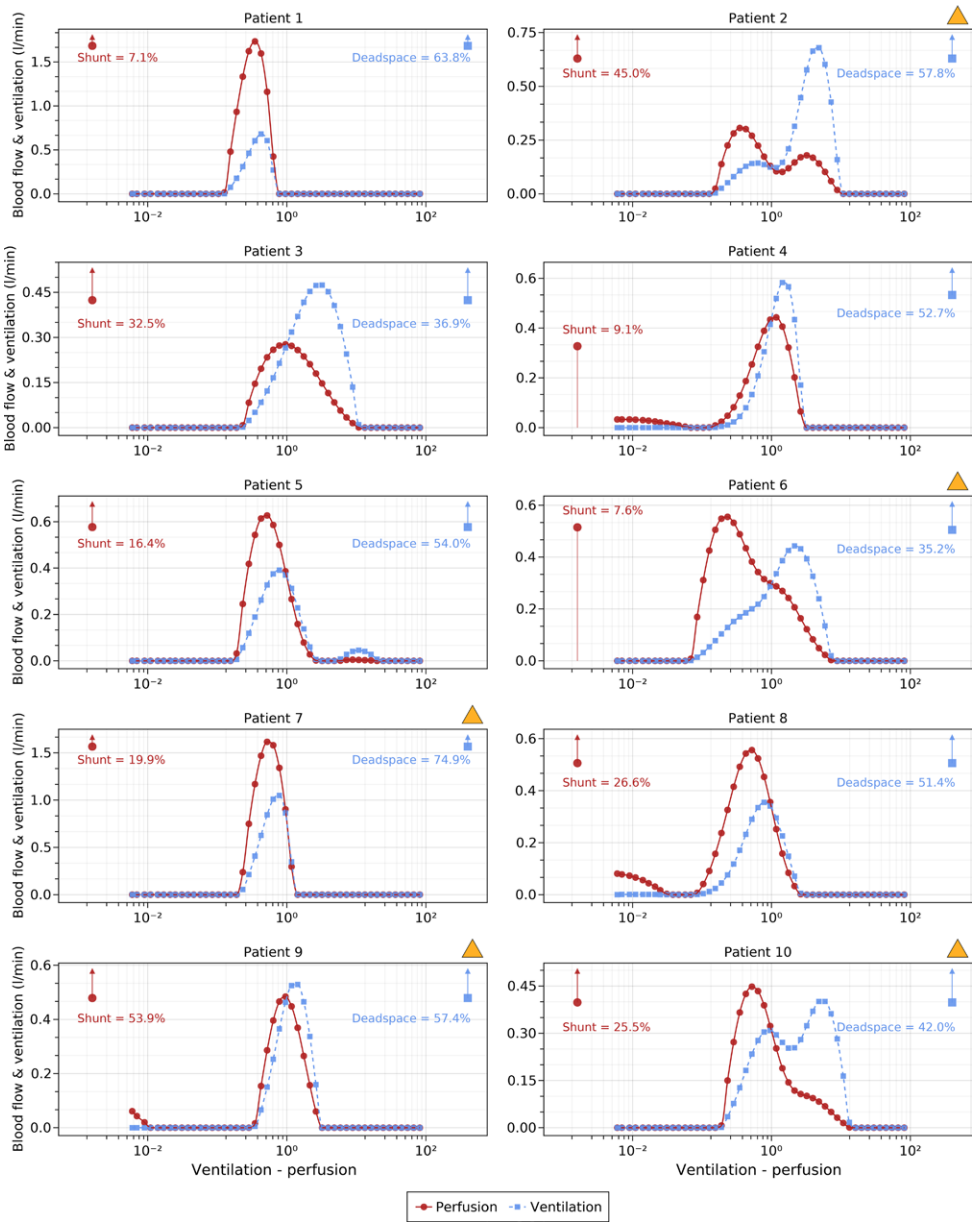

Fig. 1. Distribution of perfusion (*red*) and ventilation (*blue*) in relation to the $\dot{V}_A/\dot{Q}_T$ ratio in each of the 10 patients. Shunt ($\dot{V}_A/\dot{Q}_T = 0$) and dead space ($\dot{V}_A/\dot{Q}_T = \infty$) are represented in the *top left* and *right corners*, respectively. The *arrow* shows that both the data points are out of the represented scale. Subjects 2, 6, 7, 9, and 10 (*yellow triangle*) were radiologically diagnosed with pulmonary embolism.

LogSD, Q and LogSD,V are the second moment of perfusion and ventilation distributions, respectively. They represent the dispersion on both sides of the mean of perfusion (and ventilation) and they are therefore used as a measure to describe the heterogeneity of the distributions. Dead space was $53 \pm 11\%$, and true shunt was $25 \pm 16\%$. Table 2 summarizes these findings.

The recovered $\dot{V}_A/\dot{Q}_T$ distribution was used to calculate the predicted Pao_2 of the patient, as previously described,[16] and to estimate the degree of diffusion limitation (and of postpulmonary shunting, if present). In figure 2, the plot between the predicted Pao_2 and the measured Pao_2 shows that there was a tendency toward overestimation, suggesting the presence of diffusion limitation or postpulmonary shunting.

Anatomical Distribution of Lung Tissue and Blood Volume

Dual-energy computed tomography was used to quantify the anatomical distribution of the tissue and lung volume. The overall

Table 2. Gas Exchange Variables Acquired from MIGET

Variable	Population (n = 10)
Ventilation–perfusion	
Q_{mean}	0.65 ± 0.27
VA_{mean}	1.32 ± 0.77
LogSD, Q	0.86 ± 0.33
LogSD, VA	0.69 ± 0.25
Q_{skew}	0.48 [0.13 to 2.72]
VA_{skew}	0.19 [0.09 to 0.46]
Perfusion distribution	
$\dot{V}_A/\dot{Q}_T$ 0.001 to 0.01, %	0 [0 to 2]
$\dot{V}_A/\dot{Q}_T$ 0.01 to 0.1, %	0 [0 to 1]
$\dot{V}_A/\dot{Q}_T$ 0.1 to 1, %	56 ± 22
$\dot{V}_A/\dot{Q}_T$ 1 to 10, %	17 ± 12
$\dot{V}_A/\dot{Q}_T$ 10 to 100, %	0 [0 to 0]
Shunt, %	25 ± 16
Ventilation distribution	
$\dot{V}_A/\dot{Q}_T$ 0.001 to 0.01, %	0 [0 to 0]
$\dot{V}_A/\dot{Q}_T$ 0.01 to 0.1, %	0 ± 0
$\dot{V}_A/\dot{Q}_T$ 0.1 to 1, %	22 ± 1
$\dot{V}_A/\dot{Q}_T$ 1 to 10, %	25 ± 17
$\dot{V}_A/\dot{Q}_T$ 10 to 100, %	0 [0 to 0]
Dead space, %	53 ± 12

The data are presented as means ± SD or medians [interquartile range] as appropriate. MIGET, multiple inert gas elimination technique.

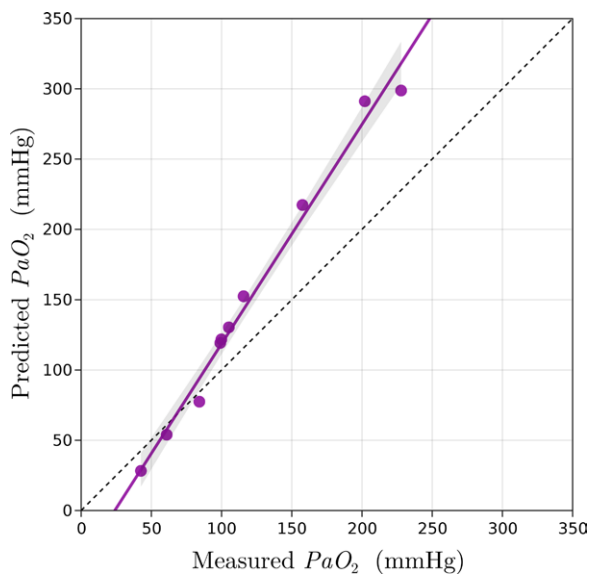

Fig. 2. Predicted *versus* measured Pao_2. The measured Pao_2 is compensated for the patient's body temperature and the barometric pressure measured on the day of the data collection. The *dashed line* represents the identity. Predicted Pao_2 = 1.6 × measured Pao_2 – 37.5 mmHg, $P < 0.001$.

lung weight was 1,427 ± 357 g,[9] and the excess tissue mass was 541.1 ± 248.4 g.[17] The blood volume maps showed the presence of defects of perfusion in all patients. Pulmonary embolism was present in five of ten patients on DECT. The distribution of the fractions of tissue mass and blood volume is displayed in figure 3A. A large fraction of the tissue volume was distributed in the range between −100 and 0 HU and above 0 HU, as expected for ARDS lungs. The blood volume, instead, was distributed across all the density compartments, with a larger fraction in the well aerated and overinflated tissue. In the overinflated and the well aerated lung compartments, we detected a relevant blood pooling (i.e., those areas were possibly overperfused). In contrast, the denser the tissue, the less the blood volume proportionally entering those areas. There was a remarkable correlation between the fraction of atelectasis (nonaerated lung tissue) and the blood volume distributed to those areas ($R^2 = 0.90$, $P < 0.001$; fig. E2, supplemental digital content, https://links.lww.com/ALN/D303). The shunt measured by MIGET was directly proportional to the fraction of atelectasis ($R^2 = 0.56$, $P = 0.012$; fig. E3a, supplemental digital content, https://links.lww.com/ALN/D303) and to the blood volume distributed to these regions ($R^2 = 0.70$, $P = 0.003$; fig. E3b, supplemental digital content, https://links.lww.com/ALN/D303). $\dot{V}_A/\dot{Q}_T$ mismatch was correlated with the fraction of blood volume distributed to the poorly aerated tissue ($R^2 = 0.54$, $P = 0.016$; fig. E4, supplemental digital content, https://links.lww.com/ALN/D303), while diffusion limitation or postpulmonary shunt was not correlated with any of the measurements we acquired. Importantly, $\dot{V}_A/\dot{Q}_T$ mismatch and diffusion limitation were not related to shunt ($P = 0.376$ and $P = 0.154$, respectively) or to each other ($P = 0.813$).

In figure 2 (B and D), we explored the relationship between the *overperfusion coefficient* as an arbitrary index of the degree of blood pooling with respect to the lung tissue and measurements of injury severity. Increasing overperfusion coefficient meant worse oxygenation, higher excess tissue mass, and worse gas exchange efficiency.[18] Of note, the coefficient was also larger in patients with pulmonary embolism (fig. 2E).

Discussion

This study describes the complex pathogenesis of hypoxemia in COVID-19 respiratory failure. A few aspects are worth mentioning.

Shunt Is the Main Cause of Hypoxemia

The past years have seen many theories speculating about the mechanisms of hypoxemia in COVID-19 patients.[19] In this study, we showed, using a state-of-the-art technique, that the main cause of hypoxemia in COVID-19 respiratory failure is shunt. This is not a new finding in ARDS; indeed, a milestone article from Dantzker *et al.*[1] and other works later[20,21] showed that shunt is the main cause of hypoxemia in ARDS from various etiologies. Despite a rather different setup (higher positive end-expiratory pressure, lower F_{IO_2}, and tidal volumes), we confirm this finding even in COVID-19–related ARDS.

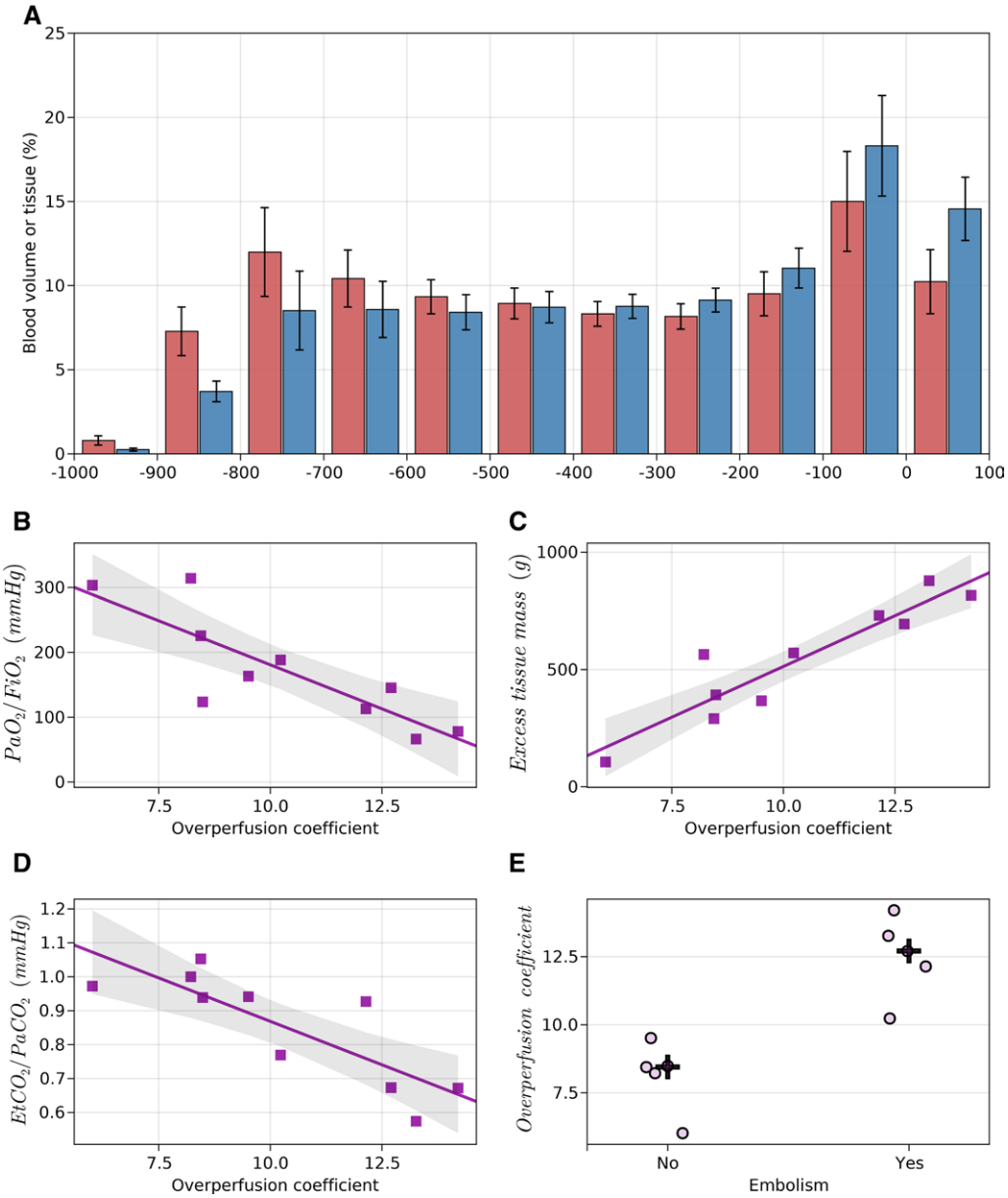

Fig. 3. (*A*) Distribution of the fractions of tissue mass (*blue*) and blood volume (*red*) across the 11 clusters of density measured at the computed tomography scan: –1,000 HU = gas, 0 HU = water. As shown, in the overinflated and the well aerated lung (from –1,000 to –500 HU), the fraction of the blood volume was larger than the fraction of tissue. The opposite was true in the atelectasis (–100 to + 100 HU). The ratio between the blood volume fraction and the tissue fraction decreased exponentially from greater than 3 in the over-inflated tissue to less than 1 in the atelectasis, crossing the value of 1 around -400 HU. (*B*) $Pao_2/Fio_2 = -27.2 \times$ overperfusion coefficient + 4,524, $R^2 = 0.66$, $P = 0.002$. (*C*) Excess tissue mass = 87 × overperfusion coefficient –353, $R^2 = 0.84$, $P < 0.001$. (*D*) $Etco_2/Paco_2 = -0.05 \times$ overperfusion coefficient + 1.38, $R^2 = 0.63$, $P = 0.004$. (*E*) Single data points of patients without (*left*) and with (*right*) pulmonary embolism. The *black cross* represents the median value.

Ventilation and Perfusion Are Mismatched

In our sample, we found that ventilation and perfusion were mismatched, mainly because more than 50% of the cardiac output was distributed in regions with a $\dot{V}_A/\dot{Q}_T$ less than 1 and greater than 0.1. Lower $\dot{V}_A/\dot{Q}_T$ regions were substantially absent. While low $\dot{V}_A/\dot{Q}_T$ can be also found in ARDS from different causes,[21] the cardiac output distributed there is usually less than 20%. The fact that $\dot{V}_A/\dot{Q}_T$ mismatch could be a more relevant cause of hypoxemia in COVID-19 has been hypothesized by our group at the beginning of the pandemic.[3,22] Later reports showed a high incidence of thromboembolic events,[23–25]

known to increase the $\dot{V}_A/\dot{Q}_T$ dispersion.[26] Our findings may indirectly confirm that the macro- and microvascular thromboembolisms typical of this disease may have a substantial effect on gas exchange.

Diffusion Limitation and Postpulmonary Shunting

A number of studies in ARDS from different etiologies firmly exclude the diffusion limitation as a mechanism for hypoxemia.[1,21] By providing a complete description of the $\dot{V}_A/\dot{Q}_T$ ratios in the lung, the MIGET allows estimating the patient's Pao_2 (*predicted* Pao_2) if that specific $\dot{V}_A/\dot{Q}_T$ distribution was solely responsible for the gas exchange. However, the actual Pao_2 (*measured* Pao_2) is also sampled directly at the bedside. The difference between the predicted and the measured Pao_2 can be considered a proxy for the magnitude of diffusion limitation. A caveat, however, is represented by the postpulmonary shunts. With this term, we refer to the shunts that occur *after* the blood has already transited across the capillary bed (mainly through bronchial and thebesian veins). After transiting through the lung, the inert gases used by MIGET do not undergo any further change in concentration. On the other hand, the blood returning from the lungs will subsequently perfuse the bronchial circulation, providing an aliquot of deoxygenated blood in the left atrium, uncoupling the exchange of oxygen from that of the inert gases. However, it has been shown that the postpulmonary shunting is of minor importance under most physiologic and pathologic conditions.[16,27]

Quite unexpectedly, we found some evidence of diffusion limitation or postpulmonary shunts in our patients. While diffusion limitation is most commonly caused by lung fibrosis,[28] it is hard to imagine that the required anatomical changes would take place so rapidly in the course of the disease (less than 7 days from intubation). Moreover, our patients were ventilated with a high FIo_2. Therefore, the postpulmonary shunting seems, in this context, more likely. Interestingly, it is known that in chronic thromboembolic disease, for example, the bronchial arteries can dilate and carry as much as 30% of the cardiac output, as a consequence of microvascular occlusions.[29,30] Recent anatomical studies have shown the opening of intrapulmonary bronchopulmonary anastomosis in COVID-19.[31] Shunting through the bronchial system could therefore explain our findings and also the positive contrast-enhanced transcranial Doppler[32] and orthodeoxia.[33] This, however, needs to be taken with care, as experimental error at multiple levels during the MIGET procedure may lead to a falsely increased difference between the measured and predicted Pao_2.

Combining Physiologic and Radiologic Findings

With DECT, we found increased lung excess tissue mass, a sign of edematous lungs, confirmed by the increased Extravascular Lung Water index. We quantitatively measured the distribution of the tissue mass and, importantly, of the blood volume. Although DECT is frequently used in various contexts, it has only recently gained popularity as an imaging technique for ARDS.[34] At the time of writing, its quantitative analysis has been performed only by a few centers.[35,36] The techniques used to evaluate the distribution of tissue and blood volume, despite small differences, are all variations of the original voxel quantitative analysis of a "traditional" CT scan.[9]

Regarding the distribution of the blood volume, it is key to understand whether hypoxic pulmonary vasoconstriction is preserved or lost.[34–36] In both healthy and diseased lungs, hypoxic pulmonary vasoconstriction diverges the blood flow away from the gasless tissue, helping maintain the matching between ventilation and perfusion.[37]

The tissue mass followed the expected distribution of ARDS lungs, with proportionally more tissue in the nonaerated regions. The blood volume followed in each interval a similar distribution, but with a tendency toward a relative hypoperfusion of the atelectasis and a relative hyperperfusion of the well aerated tissue. Importantly, the blood flowing through the atelectasis was the main determinant of shunt as measured by MIGET, confirming few other studies during both general anesthesia and ARDS.[38,39] This is relevant because it opens the way for the use of the quantitative analysis of DECT as a functional tool for the evaluation of both anatomy and gas exchange. Interestingly, we also found an association between the poorly aerated tissue (ground glass opacities) and the $\dot{V}_A/\dot{Q}_T$ mismatch, which implies that in earlier stages of the disease, when ground glass opacities are the main radiologic finding, $\dot{V}_A/\dot{Q}_T$ mismatch may play a more relevant role.

The redistribution of the blood flow away from the atelectasis, leading to hyperperfusion of the well aerated lung, is challenging to interpret. On one hand, this might represent a sign that hypoxic pulmonary vasoconstriction is working efficiently. On the other hand, when we calculated the hyperperfusion coefficient, we found an impressive association with several indices of ARDS severity, namely Pao_2/FIo_2, excess tissue mass, and $Etco_2/Paco_2$. Moreover, the coefficient was larger in patients with pulmonary embolism. This seems to support the hypothesis that the microvascular alterations[40] typical of COVID-19 may force the blood to flow through the well aerated tissue, and this redistribution might be seen as a powerful marker of severity.

Conclusions

Despite combining the complex methods of MIGET and quantitative analysis of DECT, as done here, is not likely applicable on a broader scale for clinical decision-making, these tools offer an unprecedented understanding of the mechanisms underlying this disease and ARDS in general.

However, it is important to highlight some limitations of the techniques we used. The relevant finding regarding diffusion limitation or post-pulmonary shunting is based on an adjunctive calculation on the MIGET data.

Importantly, this analysis works well when the Pao_2 is low. In our case, however, some patients had a Pao_2 close to the atmospheric one. This may lead to a rapid equilibration between air and the syringe, decreasing the measured Pao_2. Therefore, we highlight once more the need to interpret this finding with care.

Throughout the paper, when commenting on the DECT findings, we tried to avoid writing about "perfusion", preferring the wording "blood volume" instead. Indeed, DECT simply detects iodine and, through the calculation of the three material decomposition, separates a iodine map from a tissue map. Given the short duration of the acquisition, we assume iodine remains intravascular so that the distribution of iodine closely mimics the distribution of blood. Importantly, this is a volume, not a flow. While studies have found a good association between flow and volume[8], this might not be true when pulmonary capillary recruitability is compromised, which may be the case of our patients. Therefore, more than overperfusion, *blood pooling* could be likely a more appropriate wording.

The study has another obvious limitation: the low number of patients studied. However, the study also benefits from a rigorous, and until now unattempted, experimental measurement in this highly challenging context. In absence of a typical ARDS group it is difficult to generalize our findings. Nevertheless, we believe these results highlight how hypoxemia in COVID-19 is exceptionally multifactorial, combining alveolar factors, typical of ARDS, with vascular factors, more typical of macro and microembolism. Moreover, our analysis revealed a very solid correlation between some DECT-derived data and the ones derived from the much more complex MIGET. This, in our opinion, opens the door to the use of DECT in ARDS, as an interesting clinical and experimental tool.

Acknowledgments

The authors thank P.D. Wagner, M.D. (University of California, San Diego, California) for his kindness and the invaluable technical and conceptual assistance in developing MIGET at our institution. Thanks also to Alessio Gasperetti, M.D. (Johns Hopkins University, Baltimore, Maryland) for the uncompromised support during the early phases of the project. The authors are also thankful to Peter Herrmann, M.Sc. (University Medical Center, Göttingen, Germany) for his continuous assistance with the computed tomography scan data. They thank all the intensive care unit staff at the University Medical Center, Göttingen, Germany, the study nurses Loredana Benea and Andrea Kernchen, as well as the nuclear medicine (in particular, Dr. Daniel Modemann, M.Sc., for helping develop the methodology at the gas chromatography–mass spectrometry) and radiology facilities for the collaboration and compliance while performing this complex study.

Research Support

Supported by departmental sources and an unrestricted grant for respiratory medicine by Sartorius AG (Göttingen, Germany).

Competing Interests

Dr. Biggemann received a travel grant from Bayer AG (Leverkusen, Germany) and speaker fees from Bristol–Myers Squibb (New York, New York). Dr. Harnisch reports consultancy for Shionogi (Osaka, Japan). Dr. Vogt reports consultancy for MSD Merck (Rahway, New Jersey). Dr. Saager reports consultancy for the Surgical Company (Amersfoort, The Netherlands). Dr. Lotz is a board member of Röntgenfortbildung Neuss GmbH (Grevenbroich, Germany). Dr. Gattinoni reports a consultancy for SIDAM (Mirandola, Italy); he also receives lecture fees from Estor (Pero, Italy). Dr. Moerer is a member of the COVID-19-Evidenz-Oekosystem (CEOsys) Network (Germany) funded by the Federal Ministry of Education and Research; he is also a member of the national Preparedness and Pandemic Response in Deutschland (PREPARED) and Nationales Pandemie Kohorten Netz - Therapeutische Interventionsplattform (NAPKON-TIP) networks, which is funded by the Federal Ministry of Education and Research; Dr. Moerer also received honoraria for sponsored lectures by Getinge (Sweden) and Advitos GmbH (Münich, Germany) and speaker fees for workshops at the European Medical School (Oldenburg, Germany). The other authors declare no competing interests.

Correspondence

Address correspondence to Dr. Busana: University Medical Center of Göttingen, Robert-Koch Strasse 40, 37075 Göttingen, Germany. mat.busana@gmail.com. This article may be accessed for personal use at no charge through the Journal Web site, www.anesthesiology.org.

Supplemental Digital Content

Supplemental methods and results, https://links.lww.com/ALN/D303

References

1. Dantzker DR, Brook CJ, Dehart P, Lynch JP, Weg JG: Ventilation–perfusion distributions in the adult respiratory distress syndrome 14. Am Rev Respir Dis 1979; 120:1039–52
2. Ackermann M, Verleden SE, Kuehnel M, Haverich A, Welte T, Laenger F, Vanstapel A, Werlein C, Stark H, Tzankov A, Li WW, Li VW, Mentzer SJ, Jonigk D: Pulmonary vascular endothelialitis, thrombosis, and angiogenesis in COVID-19. N Engl J Med 2020; 383:120–8

3. Gattinoni L, Coppola S, Cressoni M, Busana M, Rossi S, Chiumello D: COVID-19 does not lead to a "typical" acute respiratory distress syndrome. Am J Respir Crit Care Med 2020; 201:1299–300
4. Ranieri VM, Rubenfeld GD, Thompson BT, Ferguson ND, Caldwell E, Fan E, Camporota L, Slutsky AS; ARDS Definition Task Force: Acute respiratory distress syndrome: The Berlin definition. JAMA 2012; 307:2526–33
5. Wagner PD, Saltzman HA, West JB: Measurement of continuous distributions of ventilation–perfusion ratios: Theory. J Appl Physiol 1974; 36:588–99
6. Wagner PD, Laravuso RB, Uhl RR, West JB: Continuous distributions of ventilation–perfusion ratios in normal subjects breathing air and 100 per cent O_2. J Clin Invest 1974; 54:54–68
7. Ferrer M, Zavala E, Díaz O, Roca J, Wagner PD, Rodriguez-Roisin R: Assessment of ventilation–perfusion mismatching in mechanically ventilated patients. Eur Respir J 1998; 12:1172–6
8. Fuld MK, Halaweish AF, Haynes SE, Divekar AA, Guo J, Hoffman EA: Pulmonary perfused blood volume with dual-energy CT as surrogate for pulmonary perfusion assessed with dynamic multidetector CT. Radiology 2013; 267:747–56
9. Gattinoni L, Pesenti A, Avalli L, Rossi F, Bombino M: Pressure-volume curve of total respiratory system in acute respiratory failure: Computed tomographic scan study. Am Rev Respir Dis 1987; 136:730–6
10. Cressoni M, Cozzi A, Schiaffino S, Cadringher P, Vitali P, Basso G, Ippolito D, Sardanelli F: Computation of contrast-enhanced perfusion using only two CT scan phases: A proof-of-concept study on abdominal organs. Eur Radiol Exp 2022; 6:37
11. Bezanson J, Edelman A, Karpinsky S, Shah VB: Julia: A fresh approach to numerical computing. SIAM Rev 2017; 59:65–98
12. Kamiński B, White JM, Bouchet-Valat M, Powerdistribution, Garborg S, Quinn J, Kornblith S, Cjprybol, Stukalov A, Bates D, Short T, DuBois C, Harris H, Squire K, Arslan A, Pdeffebach, Anthoff D, Kleinschmidt D, Noack A, Shah VB, Mellnik A, Arakaki T, Mohapatra T, Karpinski PS, Lin D, Chagas RAJ, Timema, ExpandingMan, Oswald F: JuliaData/DataFrames.jl: v1.5.0. 2023. 10.5281/ZENODO.7632427
13. Danisch S, Krumbiegel J: Makie.jl: Flexible high-performance data visualization for Julia. J Open Source Softw 2021; 6:3349
14. Bates D, Noack A, Kornblith S, Bouchet-Valat M, Borregaard MK, Arslan A, White JM, Kleinschmidt D, Alday P, Lynch G, Dunning I, Mogensen PK, Lendle S, Dilum Aluthge, Pdeffebach, Calderón JBS, Ayush Patnaik, Born B, Setzler B, DuBois C, Quinn J, Dutta M, Slámečka O, Bastide P, Shah VB, Blaom A, König B, Kamiński B: JuliaStats/GLM.jl: v1.8.2. 2023. 10.5281/ZENODO.7734970
15. Besançon M, Papamarkou T, Anthoff D, Arslan A, Byrne S, Lin D, Pearson J: Distributions.jl: Definition and modeling of probability distributions in the JuliaStats ecosystem. J Stat Softw 2021; 98:1–30
16. Hammond MD, Hempleman SC: Oxygen diffusing capacity estimates derived from measured $\dot{V}A/\dot{Q}$ distributions in man. Respir Physiol 1987; 69:129–47
17. Gattinoni L, Pesenti A, Bombino M, Baglioni S, Rivolta M, Rossi F, Rossi G, Fumagalli R, Marcolin R, Mascheroni D, Torresin A: Relationships between lung computed tomographic density, gas exchange, and PEEP in acute respiratory failure. Anesthesiology 1988; 69:824–32
18. Bonifazi M, Romitti F, Busana M, Palumbo MM, Steinberg I, Gattarello S, Palermo P, Saager L, Meissner K, Quintel M, Chiumello D, Gattinoni L: End-tidal to arterial PCO_2 ratio: A bedside meter of the overall gas exchanger performance. Intensive Care Med Exp 2021; 9:21
19. Gattinoni L, Chiumello D, Caironi P, Busana M, Romitti F, Brazzi L, Camporota L: COVID-19 pneumonia: Different respiratory treatments for different phenotypes? Intensive Care Med 2020; 46:1099–102
20. Pesenti A, Latini R, Riboni A, Gattinoni L: Simple estimate of the true right to left shunt (Qs/Qt) at maintenance $F1O_2$ by sulphur hexafluoride retention. Intensive Care Med 1982; 8:283–6
21. Ralph DD, Robertson HT, Weaver LJ, Hlastala MP, Carrico CJ, Hudson LD: Distribution of ventilation and perfusion during positive end-expiratory pressure in the adult respiratory distress syndrome. Am Rev Respir Dis 1985; 131:54–60
22. Busana M, Giosa L, Cressoni M, Gasperetti A, Di Girolamo L, Martinelli A, Sonzogni A, Lorini L, Palumbo MM, Romitti F, Gattarello S, Steinberg I, Herrmann P, Meissner K, Quintel M, Gattinoni L: The impact of ventilation–perfusion inequality in COVID-19: A computational model. J Appl Physiol (1985) 2021; 130:865–76
23. Wichmann D, Sperhake JP, Lutgehetmann M, Steurer S, Edler C, Heinemann A, Heinrich F, Mushumba H, Kniep I, Schroder AS, Burdelski C, Heer G de, Nierhaus A, Frings D, Pfefferle S, Becker H, Bredereke-Wiedling H, Weerth A de, Paschen HR, Sheikhzadeh-Eggers S, Stang A, Schmiedel S, Bokemeyer C, Addo MM, Aepfelbacher M, Puschel K, Kluge S: Autopsy findings and venous thromboembolism in patients with COVID-19: A prospective cohort study. Ann Intern Med 2020; 173:268–77
24. Panigada M, Bottino N, Tagliabue P, Grasselli G, Novembrino C, Chantarangkul V, Pesenti A, Peyvandi F, Tripodi A: Hypercoagulability of COVID-19 patients in intensive care unit: A report of thromboelastography

findings and other parameters of hemostasis. J Thromb Haemost 2020; 18:1738–42
25. Grasselli G, Tonetti T, Protti A, Langer T, Girardis M, Bellani G, Laffey J, Carrafiello G, Carsana L, Rizzuto C, Zanella A, Scaravilli V, Pizzilli G, Grieco DL, Di Meglio L, Pascale G de, Lanza E, Monteduro F, Zompatori M, Filippini C, Locatelli F, Cecconi M, Fumagalli R, Nava S, Vincent J-L, Antonelli M, Slutsky AS, Pesenti A, Ranieri VM.: Pathophysiology of COVID-19-associated acute respiratory distress syndrome: A multicentre prospective observational study. Lancet Respir Med 2020; 8:1201–8
26. Tsang JY, Lamm WJ, Starr IR, Hlastala MP: Spatial pattern of ventilation–perfusion mismatch following acute pulmonary thromboembolism in pigs. J Appl Physiol (1985) 2005; 98:1862–8
27. Vogiatzis I, Zakynthinos S, Boushel R, Athanasopoulos D, Guenette JA, Wagner H, Roussos C, Wagner PD: The contribution of intrapulmonary shunts to the alveolar-to-arterial oxygen difference during exercise is very small: Very small intrapulmonary shunts during exercise. J Physiol 2008; 586:2381–91
28. Agustí AGN, Roca J, Gea J, Wagner PD, Xaubet A, Rodriguez-Roisin R: Mechanisms of gas-exchange impairment in idiopathic pulmonary fibrosis. Am Rev Respir Dis 1991; 143:219–25
29. Shimizu H, Tanabe N, Terada J, Masuda M, Sakao S, Kasahara Y, Takiguchi Y, Tatsumi K, Kuriyama T: Dilatation of bronchial arteries correlates with extent of central disease in patients with chronic thromboembolic pulmonary hypertension. Circ J 2008; 72:1136–41
30. Kauczor H-U, Schwickert HC, Mayer E, Schweden F, Schild HH, Thelen M: Spiral CT of bronchial arteries in chronic thromboembolism. J Comput Assist Tomogr 1994; 18:855–61
31. Ackermann M, Tafforeau P, Wagner WL, Walsh CL, Werlein C, Kühnel MP, Länger FP, Disney C, Bodey AJ, Bellier A, Verleden SE, Lee PD, Mentzer SJ, Jonigk DD: The bronchial circulation in COVID-19 pneumonia. Am J Respir Crit Care Med 2022; 205:121–5
32. Reynolds AS, Lee AG, Renz J, DeSantis K, Liang J, Powell CA, Ventetuolo CE, Poor HD: Pulmonary vascular dilatation detected by automated transcranial Doppler in COVID-19 pneumonia. Am J Respir Crit Care Med 2020; 202:1037–9
33. Giosa L, Payen D, Busana M, Mattei A, Brazzi L, Caironi P: Orthodeoxia and its implications on awake-proning in COVID-19 pneumonia. Crit Care 2021; 25:429
34. Lang M, Som A, Mendoza DP, Flores EJ, Reid N, Carey D, Li MD, Witkin A, Rodriguez-Lopez JM, Shepard JO, Little BP: Hypoxaemia related to COVID-19: Vascular and perfusion abnormalities on dual-energy CT. Lancet Infect Dis 2020; 20:1365–6
35. Ball L, Robba C, Herrmann J, Gerard SE, Xin Y, Mandelli M, Battaglini D, Brunetti I, Minetti G, Seitun S, Bovio G, Vena A, Giacobbe DR, Bassetti M, Rocco PRM, Cereda M, Rizi RR, Castellan L, Patroniti N, Pelosi P; Collaborators of the GECOVID Group: Lung distribution of gas and blood volume in critically ill COVID-19 patients: A quantitative dual-energy computed tomography study. Crit Care 2021; 25:214
36. Perchiazzi G, Larina A, Hansen T, Frithiof R, Hultström M, Lipcsey M, Pellegrini M: Chest dual-energy CT to assess the effects of steroids on lung function in severe COVID-19 patients. Crit Care 2022; 26:328
37. Dunham-Snary KJ, Wu D, Sykes EA, Thakrar A, Parlow LRG, Mewburn JD, Parlow JL, Archer SL: Hypoxic pulmonary vasoconstriction: From molecular mechanisms to medicine. Chest 2017; 151:181–92
38. Hedenstierna G, Tokics L, Strandberg A, Lundquist H, Brismar B: Correlation of gas exchange impairment to development of atelectasis during anaesthesia and muscle paralysis. Acta Anaesthesiol Scand 1986; 30:183–91
39. Tokics L, Hedenstierna G, Svensson L, Brismar B, Cederlund T, Lundquist H, Strandberg A: $\dot{V}/\dot{Q}$ distribution and correlation to atelectasis in anesthetized paralyzed humans. J Appl Physiol 1996; 81:1822–33
40. McGonagle D, O'Donnell JS, Sharif K, Emery P, Bridgewood C: Immune mechanisms of pulmonary intravascular coagulopathy in COVID-19 pneumonia. Lancet Rheumatol 2020; 2:e437–45